Artificial Solid Electrolyte Interphase To Address the Electrochemical Degradation of Silicon Electrodes

Juchuan Li,*,[†] Nancy J. Dudney,*,[†] Jagjit Nanda,[†] and Chengdu Liang[‡]

[†]Materials Science and Technology Division and [‡]Center for Nanophase Materials Sciences, Oak Ridge National Laboratory, Oak Ridge, Tennessee 37831, United States

S *Supporting Information*

ABSTRACT: Electrochemical degradation on silicon (Si) anodes prevents them from being successfully used in lithium (Li)-ion battery full cells. Unlike the case of graphite anodes, the natural solid electrolyte interphase (SEI) films generated from carbonate electrolytes do not self-passivate on Si, causing continuous electrolyte decomposition and loss of Li ions. In this work, we aim at solving the issue of electrochemical degradation by fabricating artificial SEI films using a solid electrolyte material, lithium phosphorus oxynitride (Lipon), which conducts Li ions and blocks electrons. For Si anodes coated with Lipon of 50 nm or thicker, a significant effect is observed in suppressing electrolyte decomposition, while Lipon of thinner than 40 nm has a limited effect. Ionic and electronic conductivity measurements reveal that the artificial SEI is effective when it is a pure ionic conductor, but electrolyte decomposition is only partially suppressed when the artificial SEI is a mixed electronic–ionic conductor. The critical thickness for this transition in conducting behavior is found to be 40–50 nm. This work provides guidance for designing artificial SEI films for high-capacity Li-ion battery electrodes using solid electrolyte materials.
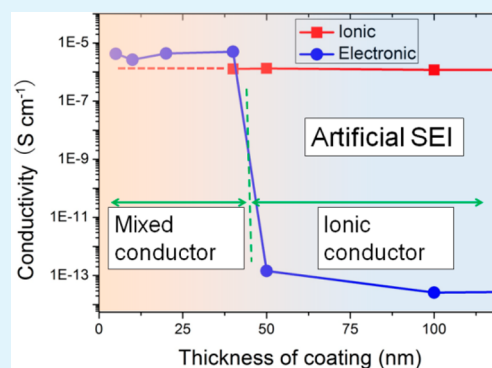
KEYWORDS: *silicon anodes, artificial solid electrolyte interphase, electrochemical degradation, solid electrolyte, lithium-ion batteries*

■ INTRODUCTION

Silicon (Si) is considered a candidate for the anodes of next-generation lithium (Li)-ion batteries (LIBs) because of its high theoretical specific capacity (4200 mAh g^{-1}), low operation potential, fast reaction kinetics, and minimal environmental impact.[1−3] However, the commercialization of Si anodes has not been realized mainly because of degradation of electrodes during cycling, including mechanical and electrochemical degradation. Numerous experimental and theoretical works have shown that the mechanical degradation of Si anodes can be remedied by reducing the characteristic size of active materials, i.e., by incorporating nanostructural Si electrodes, such as nanowires, nanotubes, hollow spheres, as well as core–shell structures.[4−11] Electrochemical degradation of Si, on the other hand, has drawn less attention, although it has been recently identified as critical for the performance of Si anodes, especially in full cells.[12−14] The operation potential of Si (below 0.5 V) is beyond the lowest unoccupied molecular orbital (LUMO) of the commercial carbonate electrolyte (about 1 V). Thus, the electrolyte undergoes reductive decomposition during lithiation of Si and forms a film consisting of organic and inorganic salts, which is usually referred as a solid electrolyte interphase (SEI) film.[15−17] Unlike the case of graphite anodes, where the SEI film is dynamically stable during electrochemical cycling,[18,19] the SEI film on Si is not electrochemically passivating.[14,20] The large volume change of Si during cycling further aggravates degradation. As a result, low

Coulombic efficiency resulting from continuous electrolyte decomposition is often observed for half-cells using Si electrodes, even when the reversible capacity is stable upon cycling.[14,21,22] Such a nonpassivating SEI film consumes Li ions and solvent from the electrolyte and limits the cycle life of LIB full cells using Si anodes.[23]

To solve the problems of unstable SEI and electrolyte reductive decomposition on Si anodes, various strategies have been developed including introducing electrolyte additives to stabilize the electrolyte/electrode interface[14,24,25] and using organic/inorganic binders[26,27] and surface coatings on Si to function as artificial SEI layers. Metal oxides such as Al_2O_3 and MoO_3, carbon, and conductive polymers have been shown to be effective coatings for Si with improved capacity retention and Coulombic efficiency.[21,22,28−31] However, the ionic and electronic transport mechanisms in such thin, few nanometer or subnanometer, coatings are not fully understood. The fact that metal oxides might react with lithium salt to form lithium metal oxyfluoride further complicates the case.[22,32,33] Ideally, the key functions of an artificial SEI include (1) transporting Li ions to realize ionic conduction, (2) blocking electrons to prevent electrochemical decomposition of the electrolyte, and (3) functioning as a physical barrier to block access of the

electrolyte to protect the electrodes from corrosion. In this regard, solid electrolyte materials, which are uniform, free of pores, ionically conducting, and electronically insulating, are the best candidates for an artificial SEI.

In this work, we demonstrate the concept of applying solid electrolyte materials as artificial SEI films to suppress electrolyte decomposition on Si anodes. Lithium phosphorus oxynitride (Lipon) is chosen to fabricate the artificial SEI because of its reasonable ionic conductivity (2×10^{-6} S cm^{-1}) and good electrochemical stability at low potential.[34] We have demonstrated that Lipon is an effective artificial SEI for several cathode materials.[35−37] In the current work, we use thin-film electrodes as a model systems to demonstrate the effect of the artificial SEI on electrochemical degradation of Si, where there is no complication brought by the binders and conducting additives. Furthermore, by using ultrathin Si films and limiting the voltage window during cycling, we eliminate the complication of mechanical degradation, which is usually coupled with electrochemical degradation in powder Si electrodes. Our results indicate that a critical thickness exists for functionalization of Lipon artificial SEI on Si anodes, and it is directly related with the ionic and electronic conductivities of Lipon.

■ EXPERIMENTAL SECTION

Amorphous Si thin films of 50 nm thick were deposited on copper foil by means of direct-current (DC) sputtering of an undoped pure Si target (99.999%, Kert J. Lesker) in pure Ar (99.9995%, Air Liquid). The power used for Si deposition was 10 W. The Lipon coating was deposited by radio-frequency magnetron sputtering of a homemade Li_3PO_4 target in a reactive N_2 (99.999%, Air Liquid) atmosphere under a power of 90 W. The thicknesses of Si and Lipon were monitored using a quartz crystal microbalance (Inficon) before and after deposition. Working electrodes with an area of 0.97 cm^2 were cut and assembled into CR2032 coin cells (Hohsen), where pure lithium metal (Alfa Aesar) foils were used as the counter electrodes. One piece of polypropylene separator (Celgard 2325) soaked with an electrolyte and an additional 50 μL electrolyte were added in each cell. The electrolyte (Novolyte) was 1 M $LiPF_6$ salt dissolved in a 3:7 volume ratio of ethylene carbonate (EC)/diethyl carbonate. Galvanostatic cycling of coin cells was conducted using a Maccor 4000 battery cycler at a rate of C/2.

Lipon thin films of desired thickness on fine lapped alumina plates (Valley Design) or glass slides (Fisher Scientific) were used for the conductivity measurement. Pure gold films of 50 nm were used as the blocking electrodes. The ionic conductivity of Lipon was measured by means of electrochemical impedance spectroscopy (EIS) using a Solartron SI 1260 impedance analyzer at room temperature (23 °C). The frequency was ramped from 10 MHz to 0.1 Hz, and the potential amplitude was 10 mV. The electronic conductivity of Lipon was determined by DC measurement of the current under potential polarization using a Bio-Logic VMP3 potentiostat with low current functions (current resolution <1 pA). The potential was ramped between −0.025 and +0.025 V with a step of 1 or 5 mV and was held at each step for up to 10 h. The stabilized current at each step was used to determine the electronic conductivity. Lipon samples were sealed in a dry Ar or N_2 atmosphere for both ionic and electronic conductivity measurements. Homemade Faraday cages were used in all experiments.

Electron microscopy images were taken using a Hitachi S-4300 microscope. Air exposure was avoided during sample transfer to minimize possible damage. X-ray photoelectron spectroscopy (XPS) was collected using a PHI 3056 XPS spectrometer with an Al Kα anode source operated at 350 W. High-resolution data were collected with a pass energy of 23.5 eV with a 0.05 eV step. Low-resolution scans were collected with a pass energy of 93.5 eV with a 0.5 eV step. The binding energy spectra were calibrated by assigning the binding

energy of C 1s (C−C) to 284.8 eV to account for charging. Samples were transferred from an Ar-filled glovebox to the XPS spectrometer using a vacuum stage.

■ RESULTS AND DISCUSSION

In this work, we investigate mainly electrochemical degradation of Si anodes and avoid the complication of mechanical degradation by choosing thin Si films of only 50 nm thick, as well as by limiting the potential window during cycling. Figure 1 shows the cycling performance of 50 nm Si cycled between 2
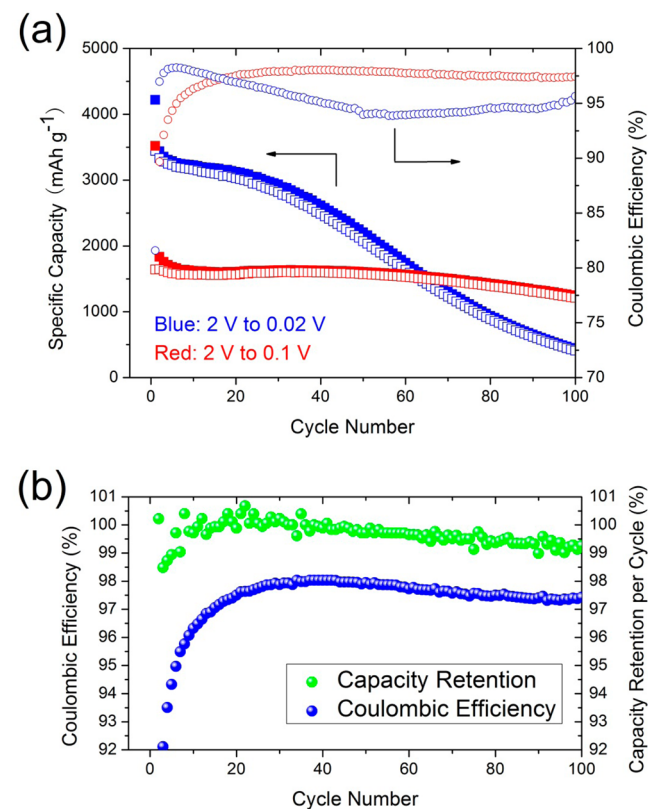

Figure 1. (a) Cycling performance of 50 nm Si film with different lower cutoff voltages. (b) Coulombic efficiency and capacity retention of Si electrodes cycled between 2 and 0.1 V. Data were obtained using half-cells.

and 0.02 V. The initial reversible capacity is 3441 mAh g^{-1} and decays steadily with extended cycling to 15% of the initial value after 100 cycles. The decay in the reversible capacity results from the loss of active material, although thin Si films generate much less cracking than thicker films.[7,38] The Coulombic efficiency stabilizes at about 95% and is a result of the combined effects of the loss of active material (mechanical degradation) and continuous SEI formation (electrochemical degradation). Consequently, it is improper to interpret these data for the purpose of quantifying electrochemical degradation. With an increased lower cutoff voltage of 0.1 V, the reversible capacity delivered by Si anodes is decreased to about 1600 mAh g^{-1}, 38% of its theoretical capacity; however, the reversible capacity is now relatively stable, as shown in Figure 1a, indicating that mechanical degradation is largely suppressed. Electrochemical degradation, i.e., the continuous formation of SEI, is not altered much by changing the lower cutoff voltage.[15−17] The strategy of limiting the voltage or capacity of the Si anode to improve its cycle life has been demonstrated

by several groups.[39−42] With a relatively stable reversible capacity, we can eliminate the effect of mechanical degradation and investigate electrochemical degradation.

The natural SEI film formed on Si anodes, which is mainly the reduction product of EC,[13,20,43] is not self-passivating, as is evidenced by a comparison of the Coulombic efficiency and capacity retention in Figure 1b. The capacity retention per cycle, defined as the ratio of the reversible capacity in the $(n + 1)^{th}$ cycle to that in the nth cycle, is larger than 99% within 100 cycles. This parameter indicates the retention of available (reversible) active materials during cycling. However, the Coulombic efficiency, which is defined as the ratio of the charge (delithiation) capacity to the discharge (lithiation) capacity in each cycle, is below 98%. The difference between the Coulombic efficiency and capacity retention is caused by the charge consumed in electrolyte decomposition. In other words, about 2% of the total charge in each cycle is consumed by the continuous formation of an SEI film. This fact indicates that natural SEI on Si in a carbonate electrolyte is not self-passivating. The more rapid decay in the Coulombic efficiency and capacity retention of Si cycled between 0.02 and 2 V is shown in Figure S1 in the Supporting Information (SI).

Building an artificial SEI film using solid electrolyte materials can suppress the capacity loss and improve the Coulombic efficiency during cycling. Although the electrolyte close to the electrode surface might still be at an unstable potential upon lithiation, electrochemical reduction reactions cannot occur because electrons are blocked from the liquid electrolyte by the artificial SEI, which is electronically insulating in nature. Also, an artificial SEI layer could potentially block solvent transportation and prevent electrochemical decomposition of the electrolyte at the interface of electrodes and artificial SEI.[44] The cycling performance of thin Si films coated with Lipon of 5−100 nm is shown in Figure 2. The capacity retention is improved by Lipon coating within the thickness range in this work; no obvious capacity decay is observed for Lipon-coated Si up to 100 cycles. The reversible capacity is lower when Lipon is 50 nm or thicker, mainly because of the additional ionic resistance contributed by Lipon, which effectively increases the lower cutoff voltage by a few millivolts. The effect of Lipon artificial SEI on the Coulombic efficiency is shown in Figure 2b. When the thickness of Lipon is below 20 nm, there is limited effect in preventing the charge loss, evidenced by the fact that the stabilized Coulombic efficiency increases slightly to about 98%. When Lipon artificial SEI is thicker than 50 nm, the Coulombic efficiency increases significantly to 99+%. The remaining loss, about 0.2−0.7%, is likely due to electrolyte corrosion of the cell hardware as well as possible residual electrolyte reduction on Lipon/Si. This observation confirms that Lipon as a solid electrolyte material can be used as an effective artificial SEI material for Si anodes. The surface morphology and XPS spectra of 100 nm Lipon-coated Si after being cycled 100 times are shown in Figures S3 and S4 in the SI.

The effect of Lipon artificial SEI can also be seen in the differential capacity−voltage profile in the first cycle. The formation of SEI in the first cycle mainly occurs between 0.7 and 0.3 V, with a reduction peak at about 0.47 V, as shown in Figure 3. With a Lipon coating of 10 or 20 nm, the intensities of the reduction peaks are reduced, but the peaks are still visible. When Lipon is thicker than 50 nm, no obvious reduction peak can be seen in Figure 3.
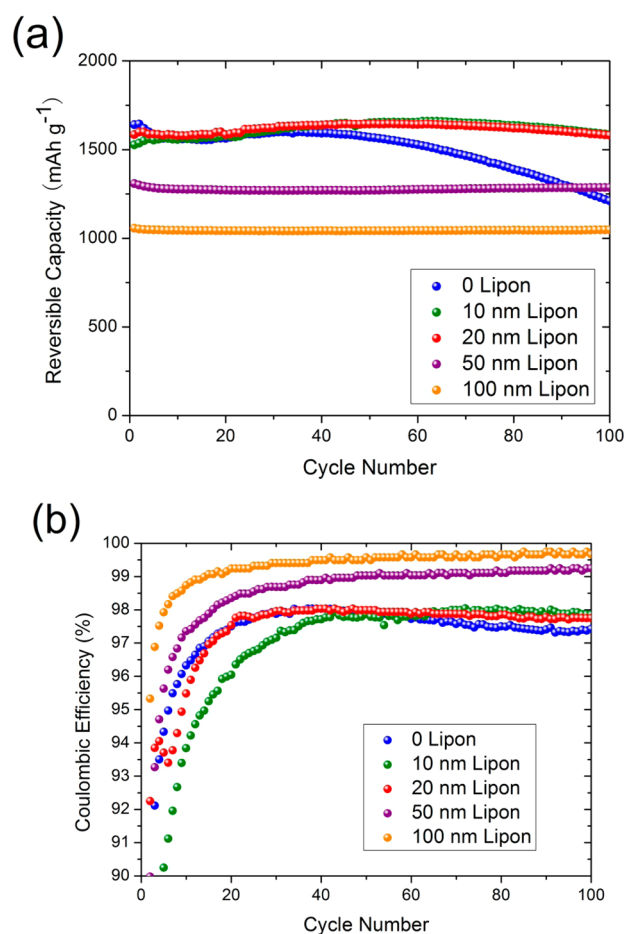

Figure 2. (a) Reversible (delithiation) capacity and (b) Coulombic efficiency as a function of the cycle number for Si coated with Lipon artificial SEI. Data were obtained using half-cells.
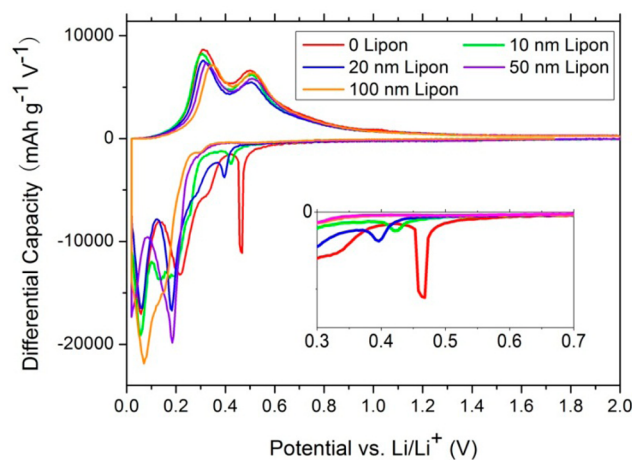

Figure 3. Differential capacity−voltage profiles of Si coated with Lipon artificial SEI in the first cycle. Si anodes were cycled between 2 and 0.02 V. The inset shows an enlarged view.

It is interesting to notice that Lipon artificial SEI films of 10 and 20 nm are not very effective because there is limited improvement in the Coulombic efficiency, although the capacity retention of Si is improved. In order to function properly as an artificial SEI, the surface coating material should minimize electron transportation. To shed more light on the

ionic and electronic conducting behavior of ultrathin Lipon, we measured these properties of Lipon using EIS and DC polarization tests. Lipon of 400 nm is chosen as a reference to represent its bulk properties. The Nyquist plots of Lipon ranging between 400 and 40 nm are shown in Figure 4. The
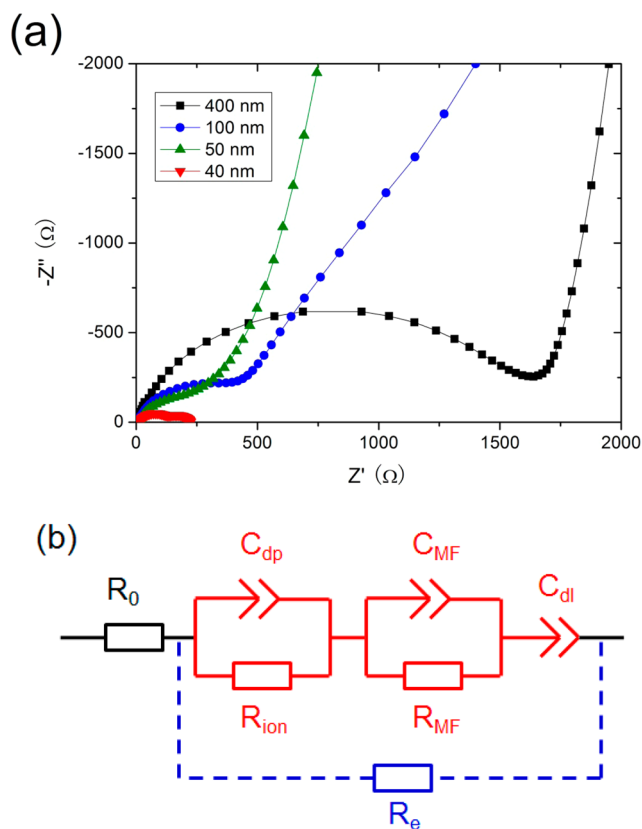

Figure 4. (a) Nyquist plot of Lipon with a thickness between 400 and 40 nm. (b) Equivalent circuit corresponding to the Nyquist plot. Red represents the ionic processes, and blue highlights the electronic conduction.

high-frequency semicircle is a result of ionic conduction and dielectric capacitance. The equivalent circuit that we use to fit the EIS data is shown in Figure 3b. Black color resistance R_0 represents the resistance of contacts and leads and corresponds to the intercept of the semicircle with the real axis at the high-frequency end. The ionic conducting processes are represented by the red components, consisting of two pairs of resistors/capacitors at high and medium frequencies (R_{ion}/C_{dp} and R_{MF}/C_{MF}), as well as a double-layer capacitance (C_{dl}) at low frequency. The electronic resistance R_e is only considered for 40 nm Lipon (see the SI for detailed discussions).

The parameters obtained from fitting of the EIS data using the equivalent circuit are summarized in Table 1, and examples of the fitting are given in Figure S5 in the SI. We use the ionic

resistance R_{ion} to calculate the ionic conductivity of Lipon. The ionic conductivity of 400 nm Lipon is found to be 1.2×10^{-6} S cm^{-1}, within the range of previously reported conductivities for Lipon.[34,45] For Lipon of 100 and 50 nm, the ionic conductivity is found to be between 1.1×10^{-6} and 1.4×10^{-6} S cm^{-1}. The deviation from ideal behavior between the high-frequency semicircle and low-frequency line is likely caused by the interfaces. It has been reported that the ceramic oxide electrolytes can be either Li-rich or Li-deficient near the interfaces, which can lead to an additional R/C circuit (R_{MF} and C_{MF}) in the EIS plots.[46,47] For 40 nm Lipon, the semicircle at low frequency is caused by electronic conduction. When Lipon is thinner than 20 nm, the samples were too conductive for EIS measurement; the ionic conductivity of Lipon is assumed to be constant. The ionic conductivity as a function of the Lipon thickness is plotted in Figure 5.
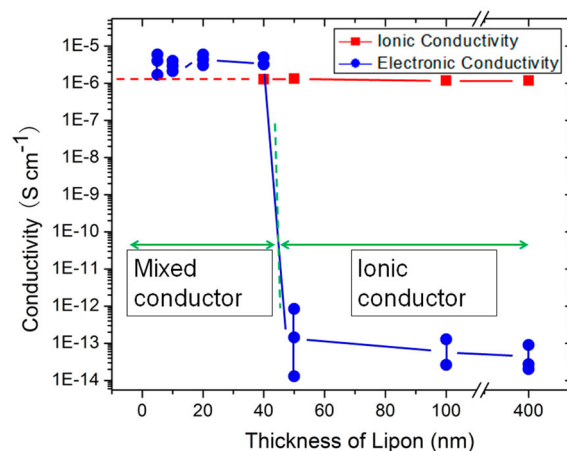

Figure 5. Electronic and ionic conductivity of ultrathin Lipon.

The electronic conductivity of Lipon is measured by DC polarization experiments and is summarized in Figure 5. Representative current−voltage curves of Lipon are shown in Figure S6 in the SI. The electronic conduction of Lipon can be divided into two regions. When Lipon is thicker than 50 nm, the electronic conductivity of Lipon is between 10^{-12} and 10^{-14} S cm^{-1}, 7 orders of magnitude lower than that of the ionic conductivity. This fact confirms that the ionic transfer number of Lipon is close to 1. When the thickness of Lipon is smaller than 40 nm, the measured electronic conductivity is about 5×10^{-6} S cm^{-1}, slightly higher than the ionic conductivity. The transition in the electronic conductivity of Lipon is similar to the tunneling behavior of ultrathin Al$_2$O$_3$[48] but at a larger thickness. The physical mechanisms are likely related with the enlarged space charge regions in heterojunctions[49] and need further study.

As summarized in Figure 5, Lipon is a mixed ionic and electronic conductor when the thickness is smaller than 40 nm

Table 1. Parameters Obtained from the Fitting of EIS Plots

thickness (nm)	R_0 (Ω)	R_{ion} (Ω)	C_{dp} (F)	R_{MF} (Ω)[a]	C_{MF} (F)[a]	C_{dl} (F)	R_e (Ω)
400	0.8	1600	1.2×10^{-8}	200	5.0×10^{-6}	1.2×10^{-6}	
100	10	400	3.2×10^{-8}	1600	1.7×10^{-6}	5.2×10^{-7}	
50	11	180	8.7×10^{-8}	500	6.9×10^{-6}	5.0×10^{-7}	
40	16	160	5.8×10^{-8}	500	1.7×10^{-6}	5.0×10^{-7}	210

[a]See the SI.

and is a pure ionic conductor when it is 50 nm or thicker. As a result, the critical thickness for Lipon to function as an effective artificial SEI, which must be pure ionic conductors, is between 40 and 50 nm.

It should be mentioned that this work focuses on demonstrating the concept of building artificial SEI using solid electrolyte materials and understanding their impact on electrochemical degradation of LIBs. Mechanical degradation of the electrodes is intentionally avoided to provide a system for this purpose. On the other hand, Lipon as an amorphous ceramic material is not likely to accommodate the huge volume expansion in powder Si electrodes. For commercial electrodes consisting of particle-type active materials, a mechanically robust artificial SEI that can accommodate the large volume change of active particles is needed.

■ CONCLUSIONS

In this work, we demonstrate the concept of fabricating artificial SEI films on Si using solid electrolyte material with an example of Lipon. Using model systems of 50 nm Si thin films and by limiting the voltage of cycling, we can examine electrochemical degradation of Si without complication from cracking in the active material. Our results show that, in order to function effectively as an artificial SEI, the Lipon coating has to reach a critical thickness. This critical thickness is found to be 40–50 nm by examining the ionic and electronic conductivities of ultrathin Lipon. Lipon is a pure ionic conductor beyond the critical thickness and is a mixed electronic–ionic conductor when thinner than the critical thickness. When thicker than 50 nm, Lipon artificial SEI on Si anodes can greatly reduce the electrolyte decomposition and irreversible capacity during cycling. The electrochemical method of screening capacity loss and the strategy of using solid electrolyte materials as artificial SEI can be applied to other LIB anodes and artificial SEI materials.

■ ASSOCIATED CONTENT

Ⓢ Supporting Information

The Coulombic efficiency and capacity retention of Si cycled between 2 and 0.02 V, cross section of 50 nm Lipon, and discussion of the ionic and electronic conductivity measurement. This material is available free of charge via the Internet at http://pubs.acs.org.

■ AUTHOR INFORMATION

Corresponding Authors
*E-mail: lij2@ornl.gov.
*E-mail: dudneynj@ornl.gov.

Notes

The authors declare no competing financial interest.

■ ACKNOWLEDGMENTS

■ REFERENCES

(1) Larcher, D.; Beattie, S.; Morcrette, M.; Edstroem, K.; Jumas, J. C.; Tarascon, J. M. Recent Findings and Prospects in the Field of Pure Metals as Negative Electrodes for Li-Ion Batteries. *J. Mater. Chem.* **2007**, *17*, 3759–3772.

(2) Park, C. M.; Kim, J. H.; Kim, H.; Sohn, H. J. Li-Alloy Based Anode Materials for Li Secondary Batteries. *Chem. Soc. Rev.* **2010**, *39*, 3115–3141.

(3) Su, X.; Wu, Q.; Li, J.; Xiao, X.; Lott, A.; Lu, W.; Sheldon, B. W.; Wu, J. Silicon-Based Nanomaterials for Lithium-Ion Batteries: A Review. *Adv. Energy. Mater.* **2014**, *4*, 1300882.

(4) Chan, C. K.; Peng, H. L.; Liu, G.; McIlwrath, K.; Zhang, X. F.; Huggins, R. A.; Cui, Y. High-Performance Lithium Battery Anodes using Silicon Nanowires. *Nat. Nanotechnol.* **2008**, *3*, 31–35.

(5) Liu, N.; Wu, H.; McDowell, M. T.; Yao, Y.; Wang, C.; Cui, Y. A Yolk–Shell Design for Stabilized and Scalable Li-Ion Battery Alloy Anodes. *Nano Lett.* **2012**, *12*, 3315–3321.

(6) He, Y.; Yu, X.; Li, G.; Wang, R.; Li, H.; Wang, Y.; Gao, H.; Huang, X. Shape Evolution of Patterned Amorphous and Polycrystalline Silicon Microarray Thin Film Electrode Caused by Lithium Insertion and Extraction. *J. Power Sources* **2012**, *216*, 131–138.

(7) Li, J.; Dozier, A. K.; Li, Y.; Yang, F.; Cheng, Y.-T. Crack Pattern Formation in Thin Film Lithium-Ion Battery Electrodes. *J. Electrochem. Soc.* **2011**, *158*, A689–A694.

(8) Liu, H.; Hu, L.; Meng, Y. S.; Li, Q. Electrodeposited Three-Dimensional Ni–Si Nanocable Arrays as High Performance Anodes for Lithium Ion Batteries. *Nanoscale* **2013**, *5*, 10376–10383.

(9) Xiao, X.; Liu, P.; Verbrugge, M. W.; Haftbaradarab, H.; Gao, H. Improved Cycling Stability of Silicon Thin Film Electrodes through Patterning for High Energy Density Lithium Batteries. *J. Power Sources* **2010**, *196*, 1409–1416.

(10) Deshpande, R.; Cheng, Y. T.; Verbrugge, M. W. Modeling Diffusion-Induced Stress in Nanowire Electrode Structures. *J. Power Sources* **2010**, *195*, 5081–5088.

(11) Wang, Y.; Wang, T.; Da, P.; Xu, M.; Wu, H.; Zheng, G. Silicon Nanowires for Biosensing, Energy Storage, and Conversion. *Adv. Mater.* **2013**, *25*, 5177–5195.

(12) Wu, H.; Chan, G.; Choi, J. W.; Ryu, I.; Yao, Y.; McDowell, M. T.; Lee, S. W.; Jackson, A.; Yang, Y.; Hu, L. Stable Cycling of Double-Walled Silicon Nanotube Battery Anodes through Solid-Electrolyte Interphase Control. *Nat. Nanotechnol.* **2012**, *7*, 310–315.

(13) Philippe, B.; Dedryvere, R.; Gorgoi, M.; Rensmo, H.; Gonbeau, D.; Edstrom, K. Improved Performance of Nano-Silicon Electrodes using the Salt LiFSi—A Photoelectron Spectroscopy Study. *J. Am. Chem. Soc.* **2013**, *135*, 9829–9842.

(14) Martin, L.; Martinez, H.; Ulldemolins, M.; Pecquenard, B.; Le Cras, F. Evolution of the Si Electrode/Electrolyte Interface in Lithium Batteries Characterized by XPS and AFM Techniques: The Influence of Vinylene Carbonate Additive. *Solid State Ionics* **2012**, *215*, 36–44.

(15) Arreaga-Salas, D. E.; Sra, A. K.; Roodenko, K.; Chabal, Y. J.; Hinkle, C. L. Progression of Solid Electrolyte Interphase Formation on Hydrogenated Amorphous Silicon Anodes for Lithium-Ion Batteries. *J. Phys. Chem. C* **2012**, *116*, 9072–9077.

(16) Nadimpalli, S. P.; Sethuraman, V. A.; Dalavi, S.; Lucht, B.; Chon, M. J.; Shenoy, V. B.; Guduru, P. R. Quantifying Capacity Loss due to Solid-Electrolyte-Interphase Layer Formation on Silicon Negative Electrodes in Lithium-Ion Batteries. *J. Power Sources* **2012**, *215*, 145–151.

(17) Philippe, B.; Dedryvère, R. m.; Allouche, J.; Lindgren, F.; Gorgoi, M.; Rensmo, H. k.; Gonbeau, D.; Edström, K. Nanosilicon Electrodes for Lithium-Ion Batteries: Interfacial Mechanisms Studied by Hard and Soft X-ray Photoelectron Spectroscopy. *Chem. Mater.* **2012**, *24*, 1107–1115.

(18) Lu, P.; Harris, S. J. Lithium Transport within the Solid Electrolyte Interphase. *Electrochem. Commun.* **2011**, *13*, 1035–1037.

(19) Harris, S. J.; Lu, P. Effects of Inhomogeneities Nanoscale to Mesoscale on the Durability of Li-Ion Batteries. *J. Phys. Chem. C* **2013**, *117*, 6481–6492.

(20) Winter, M. The Solid Electrolyte Interphase—The Most Important and the Least Understood Solid Electrolyte in Rechargeable Li Batteries. *Z. Phys. Chem. (Muenchen, Ger.)* **2009**, *223*, 1395–1406.

(21) Li, J.; Xiao, X.; Cheng, Y.-T.; Verbrugge, M. W. Atomic Layered Coating Enabling Ultrafast Surface Kinetics at Silicon Electrodes in Lithium Ion Batteries. *J. Phys. Chem. Lett.* **2013**, *4*, 3397–3391.

(22) Xiao, X. C.; Lu, P.; Ahn, D. Ultrathin Multifunctional Oxide Coatings for Lithium Ion Batteries. *Adv. Mater.* **2011**, *23*, 3911−3915.

(23) Delpuech, N.; Dupré, N.; Mazouzi, D.; Gaubicher, J.; Moreau, P.; Bridel, J.; Guyomard, D.; Lestriez, B. Correlation Between Irreversible Capacity and Electrolyte Solvents Degradation Probed by NMR in Si-Based Negative Electrode of Li-Ion Cell. *Electrochem. Commun.* **2013**, *33*, 72−75.

(24) Chen, L.; Wang, K.; Xie, X.; Xie, J. Effect of Vinylene Carbonate (VC) as Electrolyte Additive on Electrochemical Performance of Si Film Anode for Lithium Ion Batteries. *J. Power Sources* **2007**, *174*, 538−543.

(25) Profatilova, I. A.; Stock, C.; Schmitz, A.; Passerini, S.; Winter, M. Enhanced Thermal Stability of a Lithiated Nano-Silicon Electrode by Fluoroethylene Carbonate and Vinylene Carbonate. *J. Power Sources* **2012**, *222*, 140−149.

(26) Komaba, S.; Shimomura, K.; Yabuuchi, N.; Ozeki, T.; Yui, H.; Konno, K. Study on polymer binders for high-capacity SiO negative electrode of Li-ion batteries. *J. Phys. Chem. C* **2011**, *115*, 13487−13495.

(27) Menkin, S.; Golodnitsky, D.; Peled, E. Artificial Solid-Electrolyte Interphase (SEI) for Improved Cycleability and Safety of Lithium-Ion Cells for EV Applications. *Electrochem. Commun.* **2009**, *11*, 1789−1791.

(28) Wu, H.; Yu, G.; Pan, L.; Liu, N.; McDowell, M. T.; Bao, Z.; Cui, Y. Stable Li-Ion Battery Anodes by *in-situ* Polymerization of Conducting Hydrogel to Conformally Coat Silicon Nanoparticles. *Nat. Commun.* **2013**, *4*, 1943.

(29) Dillon, A.; Riley, L.; Jung, Y.; Ban, C.; Molina, D.; Mahan, A.; Cavanagh, A.; George, S.; Lee, S.-H. HWCVD MoO_3 Nanoparticles and a-Si for Next Generation Li-Ion Anodes. *Thin Solid Films* **2011**, *519*, 4495−4497.

(30) He, Y.; Yu, X.; Wang, Y.; Li, H.; Huang, X. Alumina-Coated Patterned Amorphous Silicon as the Anode for a Lithium-Ion Battery with High Coulombic Efficiency. *Adv. Mater.* **2011**, *23*, 4938−4941.

(31) Yi, R.; Dai, F.; Gordin, M. L.; Sohn, H.; Wang, D. Influence of Silicon Nanoscale Building Blocks Size and Carbon Coating on the Performance of Micro-Sized Si−C Composite Li-Ion Anodes. *Adv. Energy Mater.* **2013**, *3*, 1507−1515.

(32) Hao, S.; Wolverton, C. Lithium Transport in Amorphous Al_2O_3 and AlF_3 for Discovery of Battery Coatings. *J. Phys. Chem. C* **2013**, *117*, 8009−8013.

(33) Jung, S. C.; Han, Y.-K. How do Li Atoms Pass through the Al_2O_3 Coating Layer during Lithiation in Li-ion Batteries? *J. Phys. Chem. Lett.* **2013**, *4*, 2681−2685.

(34) Bates, J. B.; Dudney, N. J.; Gruzalski, G. R.; Zuhr, R. A.; Choudhury, A.; Luck, C. F.; Robertson, J. D. Fabrication and Characterization of Amorphous Lithium Electrolyte Thin-Films and Rechargeable Thin-Film Batteries. *J. Power Sources* **1993**, *43*, 103−110.

(35) Li, J.; Baggetto, L.; Martha, S. K.; Veith, G. M.; Nanda, J.; Liang, C.; Dudney, N. J. An Artificial Solid Electrolyte Interphase Enables the Use of a $LiNi_{0.5}Mn_{1.5}O_4$ 5 V Cathode with Conventional Electrolytes. *Adv. Energy Mater.* **2013**, *3*, 1275−1278.

(36) Kim, Y.; Veith, G. M.; Nanda, J.; Unocic, R. R.; Chi, M. F.; Dudney, N. J. High Voltage Stability of $LiCoO_2$ Particles with a Nano-Scale Lipon Coating. *Electrochim. Acta* **2011**, *56*, 6573−6580.

(37) Kim, Y.; Dudney, N. J.; Chi, M.; Martha, S. K.; Nanda, J.; Veith, G. M.; Liang, C. A Perspective on Coatings to Stabilize High-Voltage Cathodes: $LiMn_{1.5}Ni_{0.5}O_4$ with Subnanometer Lipon Cycled with $LiPF_6$ Electrolyte. *J. Electrochem. Soc.* **2013**, *160*, A3113−A3125.

(38) Haftbaradaran, H.; Xiao, X.; Gao, H. Critical Film Thickness for Fracture in Thin-Film Electrodes on Substrates in the Presence of Interfacial Sliding. *Model. Simul. Mater. Sci. Eng.* **2013**, *21*, 074008.

(39) Li, J.; Lewis, R. B.; Dahn, J. R. Sodium Carboxymethyl Cellulose—A Potential Binder for Si Negative Electrodes for Li-Ion Batteries. *Electrochem. Solid State Lett.* **2007**, *10*, A17−A20.

(40) Cui, L.-F.; Hu, L.; Wu, H.; Choi, J. W.; Cui, Y. Inorganic Glue Enabling High Performance of Silicon Particles as Lithium Ion Battery Anode. *J. Electrochem. Soc.* **2011**, *158*, A592−A596.

(41) Fridman, K.; Sharabi, R.; Elazari, R.; Gershinsky, G.; Markevich, E.; Salitra, G.; Aurbach, D.; Garsuch, A.; Lampert, J. A New Advanced Lithium Ion Battery: Combination of High Performance Amorphous Columnar Silicon Thin Film Anode, 5 V $LiNi_{0.5}Mn_{1.5}O_4$ Spinel Cathode and Fluoroethylene Carbonate-Based Electrolyte Solution. *Electrochem. Commun.* **2013**, *33*, 31−34.

(42) Mazouzi, D.; Lestriez, B.; Roue, L.; Guyomard, D. Silicon Composite Electrode with High Capacity and Long Cycle Life. *Electrochem. Solid State Lett.* **2009**, *12*, A215−A218.

(43) Xu, K. Nonaqueous Liquid Electrolytes for Lithium-Based Rechargeable Batteries. *Chem. Rev.* **2004**, *104*, 4303−4418.

(44) Pinson, M. B.; Bazant, M. Z. Theory of SEI Formation in Rechargeable Batteries: Capacity Fade, Accelerated Aging and Lifetime Prediction. *J. Electrochem. Soc.* **2013**, *160*, A243−A250.

(45) Yu, X.; Bates, J.; Jellison, G.; Hart, F. A Stable Thin-Film Lithium Electrolyte: Lithium Phosphorus Oxynitride. *J. Electrochem. Soc.* **1997**, *144*, 524−532.

(46) Yamada, H.; Oga, Y.; Saruwatari, I.; Moriguchi, I. Local Structure and Ionic Conduction at Interfaces of Electrode and Solid Electrolytes. *J. Electrochem. Soc.* **2012**, *159*, A380−A385.

(47) Ge, X.; Fu, C.; Chan, S. H. Double Layer Capacitance of Anode/Solid-Electrolyte Interfaces. *Phys. Chem. Chem. Phys.* **2011**, *13*, 15134−15142.

(48) Groner, M. D.; Elam, J. W.; Fabreguette, F. H.; George, S. M. Electrical Characterization of Thin Al_2O_3 Films Grown by Atomic Layer Deposition on Silicon and Various Metal Substrates. *Thin Solid Films* **2002**, *413*, 186−197.

(49) Sata, N.; Eberman, K.; Eberl, K.; Maier, J. Mesoscopic Fast Ion Conduction in Nanometre-Scale Planar Heterostructures. *Nature* **2000**, *408*, 946−949.

10088

dx.doi.org/10.1021/am5009419 | *ACS Appl. Mater. Interfaces* 2014, 6, 10083−10088